Separation Science and Technology
Publication details, including instructions for authors and subscription information:
http://www.informaworld.com/smpp/title~content=t713708471

Incompressible Cake Filtration of a Yield Stress Fluid

George G. Chase[a]; Patanee Dachavijit[a]
[a] Microscale Physiochemical Engineering Center, The University of Akron, Akron, Ohio, USA

Online publication date: 20 February 2003

To cite this Article Chase, George G. and Dachavijit, Patanee(2003) 'Incompressible Cake Filtration of a Yield Stress Fluid', Separation Science and Technology, 38: 4, 745 — 766
To link to this Article: DOI: 10.1081/SS-120017624
URL: http://dx.doi.org/10.1081/SS-120017624

MARCEL DEKKER, INC. • 270 MADISON AVENUE • NEW YORK, NY 10016

SEPARATION SCIENCE AND TECHNOLOGY
Vol. 38, No. 4, pp. 745–766, 2003

Incompressible Cake Filtration of a Yield Stress Fluid

George G. Chase* and Patanee Dachavijit

Microscale Physiochemical Engineering Center, The University of Akron, Akron, Ohio, USA

ABSTRACT

Filtration of Non-Newtonian fluid occurs frequently in industry. A correlation is developed by introducing the Yield Stress model in place of the Newtonian model used in the Ergun equation. The resulting model has three parameters that are functions of the geometry and roughness of the particle surfaces. Two of the parameters can be deduced in the limit as the yield stress becomes negligible and the model reduces to the Ergun equation for Newtonian fluids. The third model parameter is determined from experimental data. The correlation relates a defined friction factor to the dimensionless Reynolds and Hedstrom numbers that can be used to predict pressure drop for flow of a yield stress fluid through a packed bed of spherical particles.

This model is applied to predict incompressible cake filtration performance of a yield stress fluid. Modeling results show that for a constant pressure filtration the cake growth rate and filtrate flow rate for

*Correspondence: George G. Chase, Microscale Physiochemical Engineering Center, The University of Akron, Akron, OH 44325-3906; Fax: 330-972-5856; E-mail: gchase@uakron.edu.

DOI: 10.1081/SS-120017624 0149-6395 (Print); 1520-5754 (Online)

MARCEL DEKKER, INC. • 270 MADISON AVENUE • NEW YORK, NY 10016

the incompressible filter cake are similar to that for a Newtonian fluid, until the flow rate decreases to the level that the shear stress is not sufficient to maintain the flow. At this point the friction factor increases more rapidly than that for the Newtonian fluid, and the flow rate and cake growth rates decrease rapidly. For a given material and pressure drop the transition between Newtonian-like flow and the yield stress flow can be predicted as a function of cake height.

Key Words: Bingham plastic; Yield stress; Porous media; Cake filtration.

INTRODUCTION

Filter cakes are widely used throughout industries for a variety of purposes. Predicting pressure drop for a given flow rate is important for the design of such processes. Most recent literature in cake filtration only considers filtration of Newtonian fluids. There are several papers that describe experiments and/or models involving non-Newtonian fluids. The works by Shirato et al.[1–3] consider cake filtration of Power Law fluids. Kozicki and Kuang[4] and Kozicki and Slegr[5] evaluate the flows of viscoelastic fluids in cake filtration. In a related area Nassehi[6] models crossflow filtration by solving the Navier–Stokes equations for the fluid flowing through the porous tubes, and notes that the same approach can be applied to non-Newtonian fluids in general. Abbasov et al.[7] model particle capture in an axial magnetic filter in which the fluid is represented by a power law model. Galeczki and Galeczki[8] examine the limitations of modeling the flow of packed red blood cells through porous beds and the effect of yield shear stress.

In this paper we consider the cake filtration of a yield stress fluid. The fluid is assumed to contain rigid spherical particles of diameter d_p that are filtered out of the fluid to form the cake. The composition of yield stress fluid itself is not modeled in this work, only its observed rheological behavior. Such fluids may actually consist of very fine particles suspended in slurry whose observed net behavior is approximated by the yield stress model. In this latter case the larger particles of diameter d_p are captured in the cake while the smaller particles flow through the cake and exit in the filtrate.

To model the cake behavior we need a model for a yield stress fluid flowing through a porous material. A number of correlations are available in literature for Newtonian fluids. Ergun[9] combined the Blake–Kozeny expression, derived as a model for Newtonian flows through a bundle of capillary tubes, with an empirical Burk–Plummer relation, to obtain a packed bed model applicable to a wide range of Reynolds numbers.

Christopher and Middleman[10] introduce a modified Darcy model to represent non-Newtonian flows through porous media in which a modified permeability accounts for the non-Newtonian behavior. Park et al.[11] evaluated several approaches to modeling non-Newtonian flows through packed beds and concluded that the capillary tube approach was the best choice when combined with a particular rheological expression. Marshall and Metzner[12] discuss the effects of viscoelastic properties on flows through packed beds and the importance of the Deborah number for such fluids. Hayes et al.[13] model the flow of power law fluids through packed beds from a volume averaged approach and account for wall effects.

Pascal[14] analyzed theoretically the application of Darcy's law for flow through a porous medium to yield stress flow by introducing the effect of the yield value in the "threshold gradient." Al-Fariss and Pinder[15] applied the Herschel–Bulkley model and derived an analogous Blake–Kozeny model for the yield stress power law fluid flow through porous media at low Reynolds number. Al-Fariss and Pinder defined a modified Reynolds number that combined the yield stress with the viscous modulus for which the data collapses to a single curve. They did not extend their results to high Reynolds numbers.

In this paper the bundle of capillary tubes approach is applied to model the yield stress fluid through a porous medium similar to the approach by Al-Fariss and Pinder,[15] however our model is derived in terms of the Hedström number to account for the yield stress effect and the Reynolds number commonly used with the Ergun equation. This model is combined with the Burk–Plummer relation to obtain the analogous yield stress modified Ergun equation that spans from low to high Reynolds numbers. The correlation is fitted to experimental data to estimate one undetermined parameter, and the resulting expression is applied to model a filter cake. Furthermore, a flow–no flow condition is determined from the model, and the conditions for the transition between yield stress and Newtonian type flows are determined.

A MODIFIED ERGUN'S EQUATION FOR YIELD STRESS FLUIDS

Lets start with the Ergun equation for a Newtonian fluid flow and identify where the yield stress model must be applied. The Ergun equation most often reported in literature has the form[16]

$$\frac{P_0 - P_L}{L} = \frac{150\mu V}{d_p^2}\frac{(1-\varepsilon)^2}{\varepsilon^3} + \frac{1.75\rho V^2}{d_p}\frac{(1-\varepsilon)}{\varepsilon^3} \tag{1}$$

In deriving the Ergun equation a defined friction factor, f, proves useful. The friction factor is defined by the rate expression[16] for flow in a circular tube

$$F_k = f(2\pi RL)\left(\frac{1}{2}\rho\langle v\rangle^2\right) \tag{2}$$

where F_k is the drag force along the tube wall and $\langle v\rangle$ is the average velocity of the fluid through the tube. A force balance on the fluid over the length of the tube relates the drag force to the pressure drop along the length of the tube

$$F_k = \pi R^2(P_0 - P_L) \tag{3}$$

Combining Eqs. (2) and (3) to eliminate the drag force gives a working expression for the friction factor

$$f = \frac{R}{L}\frac{(P_0 - P_L)}{\rho\langle v\rangle^2} \tag{4}$$

For flow in the packed bed, we consider the bed to be a bundle of capillary tubes of equal diameters and equal flow rates through each tube. The total flow rate through all N capillary tubes is

$$Q = N(\pi R_{tube}^2)\langle v\rangle \tag{5}$$

Also, the total volumetric flow rate is related to the bed average velocity, V, by

$$Q = \pi R_{bed}^2 V \tag{6}$$

Eliminating the flow rates between Eqs. (5) and (6) and applying the definition of porosity gives

$$\langle v\rangle = \frac{1}{\varepsilon}V \tag{7}$$

where the porosity, ε, equals the ratio of the total volume of the capillary tubes divided by the volume of the bed.

Knowing that the bed actually consists of spherical particles of diameter d_p, and not capillary tubes, we introduce the hydraulic radius. The radius of the tubes modeled in Eq. (5) is related to the hydraulic radius by

$$R_{tube} = 2R_h \tag{8}$$

However, the hydraulic radius can also be related to the porosity and

the particle diameter as

$$R_h = \frac{\varepsilon d_p}{6(1-\varepsilon)} \tag{9}$$

Finally, combining Eq. (4), and (7–9) we get the expression for the friction factor for the packed bed in terms of the particle diameter as

$$f = \frac{\varepsilon^3 d_p}{3(1-\varepsilon)L}\frac{(P_0 - P_L)}{\rho V^2} \tag{10}$$

Equation (10) applies for all flow regimes, large or small Reynolds numbers. The Reynolds number for flow in the capillary,

$$R_e = \frac{\rho\langle v\rangle 2R_{Tube}}{\mu} \tag{11}$$

is related to the packed bed by combining Eq. (11) with (7–9) to obtain

$$R_e = \frac{\rho V d_p}{\mu}\frac{4}{6(1-\varepsilon)} \tag{12}$$

We define the Reynolds number for the packed bed as

$$R_{ep} = \frac{\rho V d_p}{\mu(1-\varepsilon)} \tag{13}$$

hence

$$R_e = \frac{2}{3}R_{ep} \tag{14}$$

For laminar flow we introduce the laminar flow friction factor correlation for the flow in a capillary.

$$f_0 = \frac{16}{R_e} \tag{15}$$

where f_0 is the friction factor value at low Reynolds number. Combining Eqs. (14) and (15) we get

$$f_0 = \frac{24}{R_{ep}} \tag{16}$$

When we eliminate the friction factor and Reynolds numbers between

Eqs. (16), (13), and (10) we obtain

$$\frac{(P_0 - P_L)}{L} = \frac{72\mu V}{d_p^2}\frac{(1-\varepsilon)^2}{\varepsilon^3} \tag{17}$$

In laminar flow, the assumption of hydraulic radius frequently gives a flow rate too large for a given pressure gradient. Hence, the number 72 is expected to be too small. Analysis of experimental data led to improvement of the formula by replacing the 72 in the denominator of Eq. (17) with 150, and yields the Blake–Kozeny equation

$$\frac{(P_0 - P_L)}{L} = \frac{150\mu V}{d_p^2}\frac{(1-\varepsilon)^2}{\varepsilon^3} \tag{18}$$

For large Reynolds numbers, a similar analysis with experimental data produced what is known as the Burke–Plummer equation, in the form

$$\frac{(P_0 - P_L)}{L} = 1.75\frac{1}{d_p}\rho V^2\frac{1-\varepsilon}{\varepsilon^3} \tag{19}$$

Combining Eqs. (19) and (10) yields the friction factor for large Reynolds numbers to be

$$f_\infty = 0.5833 \tag{20}$$

Ergun[9] found that by adding Eqs. (18) and (19) we obtain a correlation for the full range of flows, as given in Eq. (1). This is equivalent to summing the two asymptotic solutions to obtain the friction factor for the full range of Reynolds numbers as

$$f = f_0 + f_\infty \tag{21}$$

MacDonald et al.[17] extended Ergun's results to a wider range of materials and found that the correlation is improved by replacing the 150 in Eq. (1) with 180, and by replacing the 1.75 with 1.8 for smooth particles or by 4.0 for rough particles. In this work we only consider the smooth particles, hence Eq. (1) is revised and the Ergun equation for Newtonian fluids becomes

$$\frac{P_0 - P_L}{L} = \frac{180\mu V}{d_p^2}\frac{(1-\varepsilon)^2}{\varepsilon^3} + \frac{1.80\rho V^2}{d_p}\frac{(1-\varepsilon)}{\varepsilon^3} \tag{22}$$

For comparison with non-Newtonian fluids it is more convenient to express the correlation in the form of Eq. (21). Taking into account the refinement by MacDonald et al.,[17] the functional forms for the Low and High

Reynolds Number friction factors are

$$f_0 = \frac{C_1}{R_{ep}} \quad \text{where} \quad C_1 = 60 \tag{23}$$

$$f_\infty = C_2 \quad \text{where} \quad C_2 = 0.6 \tag{24}$$

Hence, one can model the pressure drop for a Newtonian fluid flowing through a packed bed using the Ergun equation in the form of Eq. (22), or one can calculate the friction factor through Eqs. (21), (23), and (24), and then calculate the pressure drop using the definition of the friction factor, in Eq. (10). For Newtonian fluids, Eq. (22) is more direct. For the yield stress fluid it turns out that the second method, calculating the friction factor first, is the most convenient approach.

Following a similar approach for a yield stress fluid flow requires (1) a laminar flow correlation for yield stress fluids in a tube, (2) asymptotic assumptions that as the yield stress goes to zero (or when the Reynolds number becomes very large), the solution collapses to the Newtonian fluid correlation, and (3) an expression for when the fluid will not flow.

The yield stress model for flow in a tube has the form

$$\tau_{rz} = -\mu_o \frac{dv_z}{dr} \pm \tau_o \quad \text{for} \quad |\tau_{rz}| > \tau_o$$

$$\frac{dv_z}{dr} = 0 \quad \text{for} \quad |\tau_{rz}| < \tau_o \tag{25}$$

The low Reynolds number laminar flow solution for a yield stress fluid flowing in a tube is[16]

$$\pi R_{tube}^4 \langle v \rangle = \frac{\pi (P_0 - P_L) R_{tube}^4}{8 \mu_o L} \left[1 - \frac{4}{3} \left(\frac{\tau_o}{\tau_R} \right) + \frac{1}{3} \left(\frac{\tau_o}{\tau_R} \right)^4 \right] \tag{26}$$

where τ_R is the shear stress value at the tube wall.

Equation (26) contains the fluid yield stress parameter, τ_o. The dimensionless group that represents the yield stress is the Hedstrom number. For flow of a yield stress fluid in a packed bed the Hedstrom and Reynolds

numbers are defined as

$$H_{ep} = \frac{\tau_o \rho d_p^2}{\mu_o^2} \frac{\varepsilon^2}{(1-\varepsilon)^2} \tag{27}$$

$$R_{ep} = \frac{\rho V d_p}{\mu_o (1-\varepsilon)} \tag{28}$$

Combining Eqs. (7–10), and (26–28), with some algebraic rearrangement, we derive the low Reynolds number friction factor value to be

$$f_0 = \frac{24}{R_{ep}} \left[1 - \frac{4}{3} \left(\frac{2H_{ep}}{f_0 R_{ep}^2} \right) + \frac{1}{3} \left(\frac{2H_{ep}}{f_0 R_{ep}^2} \right)^4 \right]^{-1} \tag{29}$$

The assumption of hydraulic radius is expected to make the numerical values of 24 and 2 in Eq. (29) to be too small, as in the case with the Newtonian fluid. Those constants are replaced with constants C_1 and C_3, to be determined.

$$f_0 = \frac{C_1}{R_{ep}} \left[1 - \frac{4}{3} \left(\frac{C_3 H_{ep}}{f_0 R_{ep}^2} \right) + \frac{1}{3} \left(\frac{C_3 H_{ep}}{f_0 R_{ep}^2} \right)^4 \right]^{-1} \tag{30}$$

Since the effect of the yield stress diminishes as Reynolds number becomes very large (i.e. for large strain rates), the yield stress fluid behaves similar to a Newtonian fluid at large Reynolds number. Hence, for large Reynolds numbers, the friction factor becomes

$$f_\infty = C_2 \tag{31}$$

Following Ergun's approach, the friction factor for the full flow range takes the form of Eq. (24) where the constants C_1, C_2, C_3 in Eqs. (30) and (31) must be determined.

In the limit as $\tau_o \to 0$, Eq. (30) must reduce to the Newtonian fluid correlation, Eq. (21). Hence by inspection we conclude $C_1 = 60$ and $C_2 = 0.6$ for smooth particles. For rough particles $C_2 = 1.33$ as determine by MacDonald et al.[17] The constant, C_3, must be determined empirically from experiments with yield stress fluids (the topic of the next section).

The inequality condition in the yield stress model, Eq. (25), suggests that if the applied pressure is not large enough, no flow will occur. For flow in a tube this occurs when $\tau_0/\tau_R < 1$. This ratio appears on the right side of Eq. (26) and by inspection with Eq. (29), the equivalent requirement for flow is

$$\frac{C_3 H_{ep}}{f R_{ep}^2} < 1 \tag{32}$$

In measurable quantities, flow occurs when the condition

$$\frac{(P_0 - P_L)}{L} > \frac{3C_3\tau_o}{d_p}\frac{(1-\varepsilon)}{\varepsilon} \tag{33}$$

is satisfied.

EXPERIMENTAL DETERMINATION OF PARAMETER C_3

A true yield stress fluid behavior is difficult to produce in a laboratory. However, a number of fluid mixtures give an approximate yield stress behavior. One such fluid, as reported by Wünsch,[18] is an aqueous solution of Carbopol 941 (BF Goodrich Corporation). Solutions with concentrations varying between 0.15 to 1.3 mass percent of Carbopol 941 by mass are used to determine the parameter C_3. All rheological measurements are for the mixtures at room temperature. The rheological parameters for characterizing the fluid are determined from shear stress—shear rate data measured by a Dynamic Stress Rheometer by Rheometric Scientific, Inc.

In the packed bed experiments the aqueous solutions of known concentrations of Carbopol 941 are pumped through a packed column of glass beads in the experimental setup shown in the diagram in Fig. 1. The pressure drop is measured over a range of flow rates for each concentration. The packed column is a Plexiglas tube of 5.7 cm in inside diameter and 110 cm in length. The spherical glass beads have a narrow size distribution with a number-average diameter of 0.211 cm, as determined by microscopic measurement. The tube wall taps for pressure measurements are 87 cm apart and two tube diameters from the ends of the packed bed to minimize entrance and exit effects. The column, fluid reservoir, and flow meter are mounted vertically and fitted with pipes and valves to allow upward flow for filling and downward flow for testing. Air pressure is used to drive the flow.

The bed porosity is calculated from Ergun's Equation, Eq. (1), with pressure drop and flow rate data of distilled water flowing through the packed column. The calculated porosity of 0.37 agrees with reported values of beds with normal packed spherical particles.[19]

The data in Fig. 2 are obtained by least-squares fitting of the stress–strain rate data to obtain μ_o and τ_o from the slope and intercept of the fitted linear curves. The data in Fig. 2 in turn are fitted by least squares fit to obtain the values of μ_o and τ_o as functions of concentration. The values from these fitted curves are used in the packed bed analysis below.

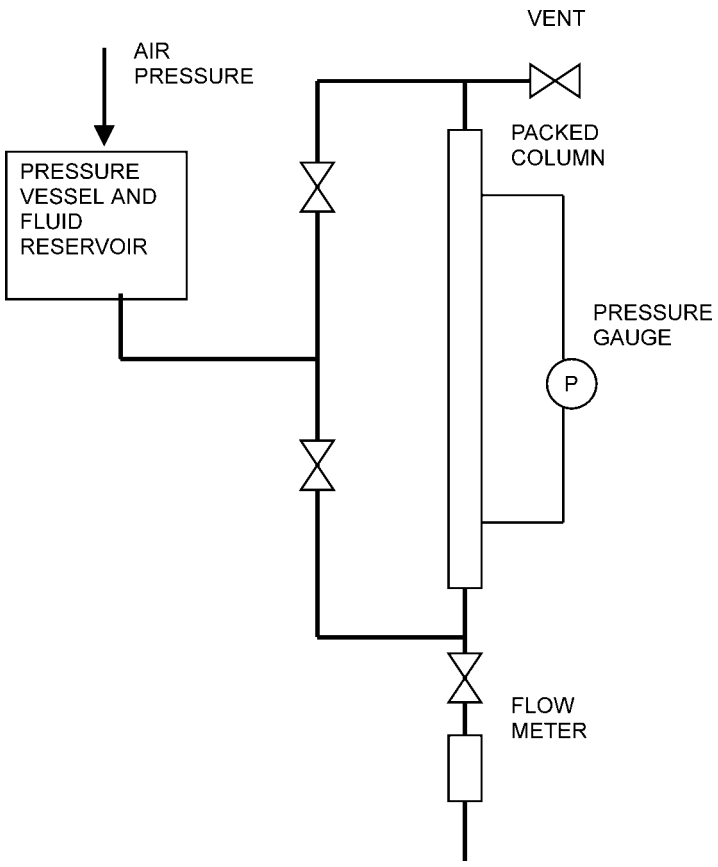

Figure 1. Schematic of the packed column experiment. Air pressure drives the fluid flow. For filling the column with fluid, the valves are positioned to drive the flow upward to vent air out of the top. In the experiments the flow is driven downward through the column and the flow meter while pressure drop and flow rate are monitored.

The value of C_3 is determined by minimizing the error between the experimental and calculated pressure drop data in the packed bed experiments, shown in Fig. 3. The results in Fig. 3 give a relatively good fit of the experimental data over a range of pressures, flow rates, and material parameters. The value of $C_3 = 3.50$ is also remarkably close to the value of 2 predicted using the bundle of capillary tubes model, as shown in Eq. (29). This result is tentative. More experimental data should be obtained for several different materials to determine the optimal value for C_3.

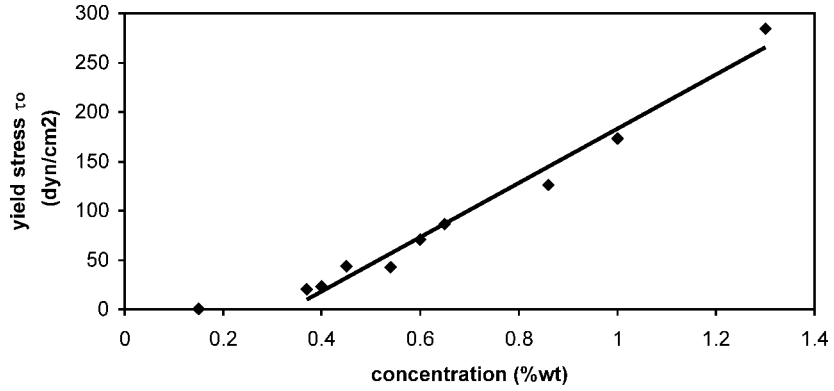

(a)

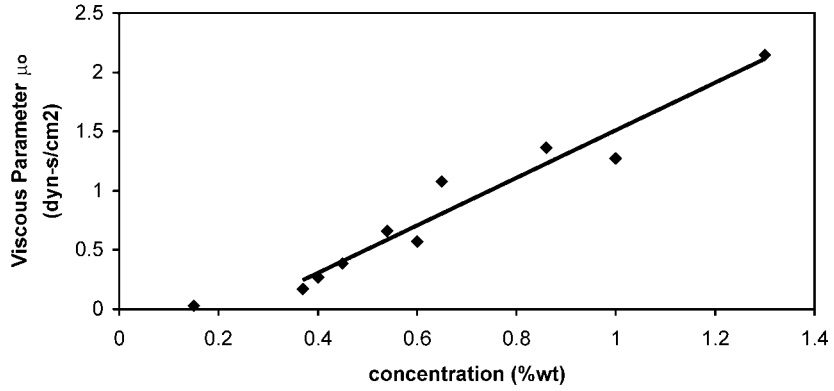

(b)

Figure 2. (a) Yield stress, τ_o, versus concentration. (b) Viscosity parameter, μ_o, versus concentration of carbopol in aqueous solution. The discrete data points are the experimental μ_o and τ_o values. The solid curves are the least squares fitted values as a function of concentration and are used in the packed bed analysis. The regression coefficient for the curve in (a) is $R^2 = 0.975$ and for (b) is $R^2 = 0.954$.

Using this value for C_3 the friction factor may now be calculated as a function of velocity using Eqs. (21), (27), (28), (30), and (31), where $C_1 = 60.0$, $C_2 = 0.60$, and $C_3 = 3.50$. The pressure drop follows from the friction factor and Eq. (10). However, Eq. (30) is difficult to use to predict the friction factor and pressure drop because of its implicit dependence on f_0. To plot the results in a more convenient form, Eq. (30) is rearranged in order to eliminate

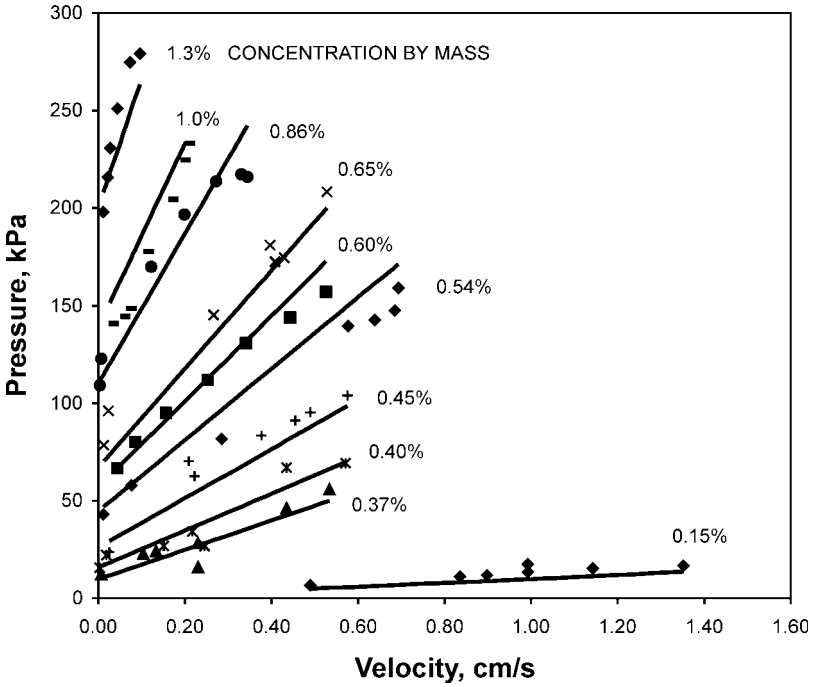

Figure 3. Pressure drop versus velocity data for flow of a yield stress fluid in a packed bed. The discrete points are experimentally measured data points. The curves are calculated values for $C_3 = 3.50$ and the yield stress model parameters, τ_0 and μ_0, determined from the fitted values listed in Table 1. The concentrations are the mass fractional amounts of Carbopol 941 in aqueous solution.

the friction factor in the denominator.

$$f_0 = \left[\left(\frac{C_1}{\mathrm{Re}_p} + \frac{4}{3} \frac{C_3 He_p}{\mathrm{Re}_p^2} \right) f_0^3 - \frac{1}{3} \left(\frac{C_3 He_p}{\mathrm{Re}_p^2} \right)^4 \right]^{0.25} \tag{34}$$

The Reynolds and Hedström numbers are calculated via Eqs. (27) and (28). A method of successive substitution is used to calculate f_0 from Eq. (34) from an initial guess and for fixed values of R_{ep} and H_{ep}. Since Eq. (34) is fourth order in f_0, the polynomial has four roots, of which two are negative and two are positive. The negative values can be discarded because the friction

factor cannot be negative. Of the two positive values, one is larger than the corresponding value for Newtonian fluids and one is near zero. The correct root is greater than the value for the Newtonian fluid.[20]

The friction factor is plotted in Fig. 4 as a function of R_{ep} and H_{ep}. This correlation may be used to calculate the friction factor and the pressure subsequently calculated via Eq. (10). With this plot the pressure drop is easily calculated without the iterative calculations required by Eq. (34). The criteria given in Eq. (33) determines when flow occurs.

This correlation does not take into account the particle size distribution or shape, both of which are known to affect the accuracy of the Ergun equation to predict Newtonian fluid flow through a packed bed. These topics are left for future work. Furthermore, the value for parameter C_3 is based on limited data and requires further study.

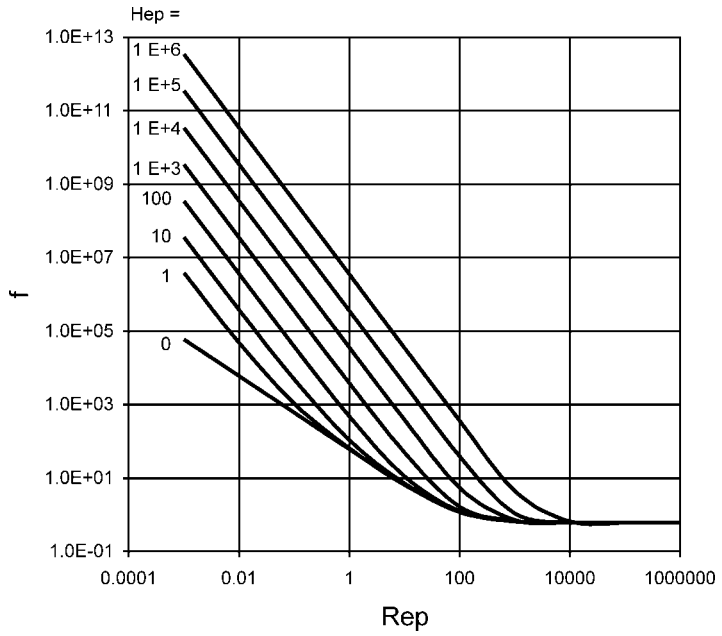

Figure 4. Friction factor plot for yield stress fluid flow through a packed bed. The friction factor is plotted from Eqs. (32)–(34) and for values $C_1 = 60.0$, $C_2 = 0.60$, and $C_3 = 3.50$. The curve for $H_{ep} = 0$ is equivalent to the Ergun equation for a Newtonian fluid.

MODELING OF CAKE FILTRATION OF A YIELD STRESS FLUID

Volume Averaging theory provides a set of continuum equations that describe the conservation laws of mass, momentum, energy, and entropy in a porous medium.[21–25] It is assumed here that the flows are isothermal and that all of the effects of interest for cake filtration are contained in the momentum and mass balances. Furthermore, it is assumed that there are only two phases (designated '*s*' for solid and '*f*' for fluid), there are no chemical reactions, and no mass transfer between the phases. The mass and momentum balances are:

α—Phase Mass

$$\frac{\partial}{\partial t}(\varepsilon^{\alpha}\rho^{\alpha}) + \underline{\nabla}\cdot(\varepsilon^{\alpha}\rho^{\alpha}\underline{v}) = 0 \quad \text{for} \quad \alpha = s,f \tag{35}$$

f—Phase Momentum

$$\frac{\partial}{\partial t}(\varepsilon^{f}\rho^{f}\underline{v}^{f}) + \underline{\nabla}\cdot(\varepsilon^{f}\rho^{f}\underline{v}^{f}\underline{v}^{f}) + \varepsilon^{f}\underline{\nabla}P^{f} + \underline{\nabla}\cdot\underline{\underline{\tau}}^{f} - \varepsilon^{f}\rho^{f}\underline{g} + \underline{F}^{d} = 0 \tag{36}$$

s—Phase Momentum

$$\frac{\partial}{\partial t}(\varepsilon^{s}\rho^{s}\underline{v}^{s}) + \underline{\nabla}\cdot(\varepsilon^{s}\rho^{s}\underline{v}^{s}\underline{v}^{s}) + \varepsilon^{s}\underline{\nabla}P^{f} + \underline{\nabla}\cdot\underline{\underline{\tau}}^{s} - \varepsilon^{s}\rho^{s}\underline{g} - \underline{F}^{d} = 0 \tag{37}$$

We make the additional assumptions that the intrinsic mass densities for each phase, ρ^{f} and ρ^{s}, are constant, and the flow is one-dimensional in the z-direction. From dimensional analysis the inertial forces and the fluid phase wall shear stress are neglected compared to the pressure, drag, solid matrix normal stress, and the gravity forces.[26] We also assume that the solid phase matrix is incompressible. For cake filtration this latter assumption implies that the solid phase has a zero velocity within the filter cake and that the porosity is uniform and constant.

These assumptions significantly simplify the mass and momentum balances. For the fluid phase the mass and momentum balances become

f—Phase Mass

$$\frac{\partial}{\partial z}(v_{z}^{f}) = 0 \tag{38}$$

f—Phase Momentum

$$\varepsilon^f \frac{\partial P}{\partial z} + F_z^d = 0 \quad \text{where} \quad P = P^f + \rho^f g_z z \tag{39}$$

The solid phase balances are identically zero for this case. Additional relations include

$$\varepsilon^f + \varepsilon^s = 1 \tag{40}$$

$$V = \varepsilon^f v_z^f \tag{41}$$

where V is the approach velocity. Furthermore, the fluid phase volume fraction, ε^f, is the same as the cake porosity, ε, and the fluid phase intrinsic density, ρ^f, is the same as ρ as used in the Ergun equation, which simplifies the notation.

For mathematical closure of Eqs. (38) and (39) we need a constitutive relation for the drag force, F_z^d. To deduce a plausible constitutive correlation for a yield stress fluid, we rearrange Eq. (10) to obtain

$$\frac{P_o - P_L}{L} = \frac{3f(1-\varepsilon)\rho V^2}{\varepsilon^3 d_p} \tag{42}$$

In the limit as $L \rightarrow$ *small* the pressure drop term on the left-hand side of Eq. (42) reduces to the gradient in the pressure, while the right-hand side is not affected. This gives

$$-\frac{\partial P}{\partial z} = \frac{3f(1-\varepsilon)\rho V^2}{\varepsilon^3 d_p} \tag{43}$$

Comparison of Eqs. (43) and (39) provides the desired relationship for the drag force

$$F_z^d = \frac{3f(1-\varepsilon)\rho V^2}{\varepsilon^2 d_p} \tag{44}$$

This relationship is independent of whether the fluid is Newtonian or Yield Stress. The friction factor correlation accounts for the fluid type.

Deriving the relation for the drag force in Eq. (44) is straight forward for the incompressible cake modeling that follows. However, it is more complicated if compressive filter cakes are to be modeled.[27] For compressive filter cakes a constitutive correlation relating the stress on the solid phase, $\underline{\underline{\tau}}^s$, to the porosity is needed. The latter results in a change in porosity with position, which in turn through Eq. (44) will make the drag force vary with position.

Combining Eqs. (44) and (39) and integrating from $z = 0$ to an arbitrary position z gives the pressure profile

$$P(z,t) = P_o - \frac{3f(1-\varepsilon)\rho V^2}{\varepsilon^3 d_p} z \tag{45}$$

which shows the pressure profile is linear at each instant in time. If we evaluate Eq. (45) at $z = L$, we get back Eq. (42). We use these equations to model the filter cake.

The material properties are listed in Table 1 for all of these simulations. The slurry is assumed to be made up of 100 micron rigid spherical particles, that upon filtration form the filter cake. The slurry fluid phase volume fraction is used later to calculate the cake growth rate.

We consider a constant pressure filtration where the pressure drop is fixed at 1000 kPa. Equations (42) or (45) require an infinite flow rate at the start when the cake depth is zero. Hence, we assume that the filter medium imparts a resistance to flow equivalent to a 1 mm thickness of the cake. The medium and cake pressure drops are summed to give the constant pressure drop of 1000 kPa. In Fig. 5 are plots of the approach velocity versus cake depth for different values of the Hedstrom number.

In the calculations for Fig. 5 the friction factor values used in Eq. (42) are determined from the correlation in Fig. 4. For cakes less than 0.1 m in depth and Hedstrom numbers less than about 100 the fluids behave as a Newtonian fluid, with the Reynolds numbers large enough that the friction factor is read from the lower part of the curve in Fig. 4. For larger Hedstrom numbers a transition point occurs at which the friction factor is read from the upper curves in Fig. 4. At this transition the velocity drops dramatically.

When we apply a mass jump balance at the top of the cake[25] we can derive

$$\frac{1}{G}\int_0^{L(t)} \frac{dL}{V} = t \tag{46}$$

which can be numerically integrated to relate the cake height as a function of time.

Table 1. Material properties in filter cake model.

Fluid Density, ρ, kg m^{-3}	1000
Viscosity, μ and μ_o, kg m^{-1} s^{-1}	0.001
Cake porosity (fluid phase volume fraction), ε	0.4
Slurry fluid phase volume fraction, ε^f_{slurry}	0.95
Particle diameter, d_p, m	0.0001

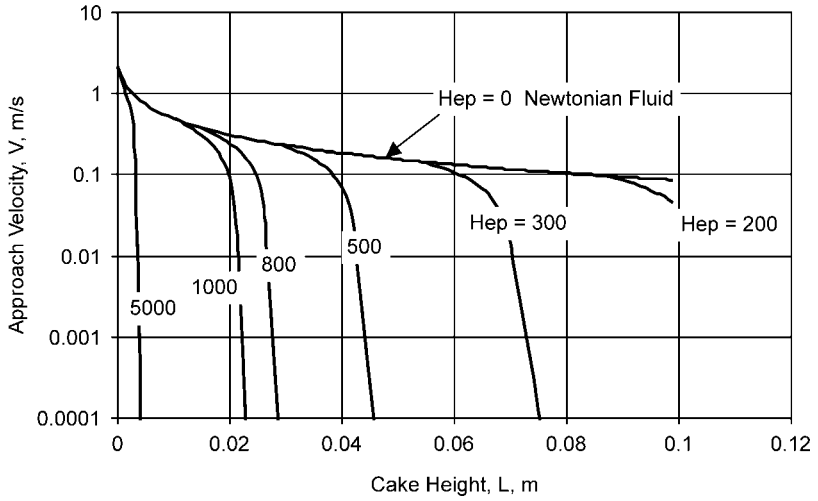

Figure 5. Comparison of velocities versus bed depth for the material properties listed in Table 1 and constant pressure drop of 100 kPa over the cake and medium. When the cake is small the velocities are large enough that the friction factor from Fig. 4 coincides with that for a Newtonian fluid. As the cake builds up, a point is reached at which the Reynolds number is small enough (for the particular value of the Hedstrom number) and the friction factor follows the upper curves in Fig. 4. As the cake size increases further the velocity dramatically decreases. The cake depth at which this occurs depends upon the Hedstrom number value.

In this expression G is cake volume to filtrate volume ratio and is given by[28]

$$G = \frac{1 - \varepsilon^{f}_{slurry}}{\varepsilon^{f}_{slurry} - \varepsilon} \tag{47}$$

Using Eq. (47) we plot in Fig. 6 the calculated values for cake height versus filtration time. In Fig. 6 the cake growth rate appears to accelerate with time as the cake depth gets larger. However the time scale is plotted as the logarithm of time, which compresses the time scale and gives this appearance. The cake growth rate is actually decreasing in time as the cake depth increases. All of the plots initially follow the curve obtained for a Newtonian fluid, until the transition occurs and the velocity decreases. The rate of cake growth, as indicated by the shape of the curves, drops significantly after the transition occurs to low Reynolds number.

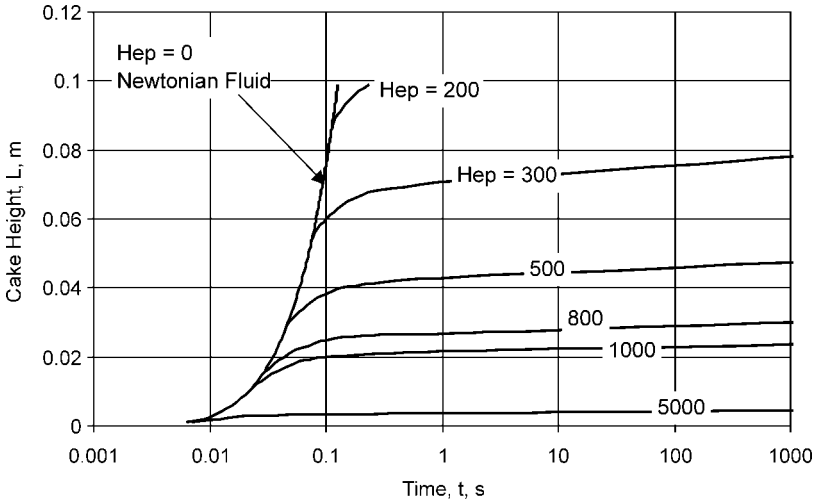

Figure 6. Cake height as a function of time. Each cake height versus time starts out following the same rate as would a Newtonian fluid. When the Reynolds number decreases to the point that the friction factor deviates from that for a Newtonian fluid in Fig. 4 then the flow rate decreases dramatically. This causes the rate of cake growth to decrease, as shown by the curves marked for various Hedstrom number values.

The yield stress fluid has a criteria for flow, as given in Eqs. (32) and (33). This limit is plotted in Fig. 7 for the material properties assumed in the simple case modeled here. The limiting cake height at which flow stops may not be practical to reach for most applications because the flow will have reduced to very small values prior to reaching that height. In most filtrations operators may wish to stop the filtration at the transition point to avoid the unnecessarily long filtration times that would occur. An approximate curve fitted relation for this transition point is given by

$$R_{ep} = 0.0897 H_{ep}^{0.979} \tag{48}$$

From Eq. (48) the velocity may be calculated from the Reynolds number and from the velocity the cake height may be calculated using Eq. (42). This transition line is also plotted in Fig. 7.

In Fig. 7 the flow–no flow line separates the plot, as determined by Eq. (33), into a flow region and a no-flow region. The no-flow region occurs above the flow–no flow line. The flow region is further divided into a yield stress region and an Ergun equation region. The yield stress region coincides with the friction factor determined from the upper curves in Fig. 4 and the Ergun

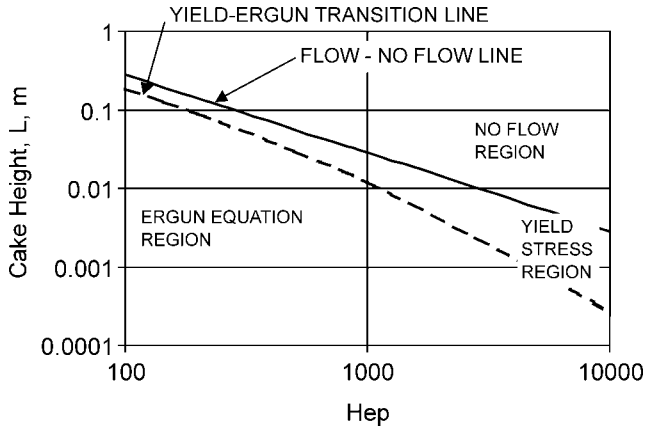

Figure 7. Plot of cake depth vs. yield stress, for the material properties in Table 1, and for a constant pressure of 1000 kPa. Flow will not occur in the no-flow region above the flow–no flow line. The flow region below this line is divided into a yield stress region and an Ergun equation region. The transition line between the yield stress region and the Ergun equation region is determined as the point at which the friction factor starts to deviate from the zero Hedstrom number curve in Fig. 4.

equation region coincides with the friction factor corresponding to the values as given by the Ergun equation for a Hedstrom number of zero. In the yield stress region the flow rate decreases dramatically from flow rate coinciding with the Ergun equation region, as is shown in Fig. 5.

CONCLUSIONS

In this work, a correlation for the friction factor for flow of a yield stress fluid through a packed bed is derived. This correlation has three parameters, two of which are determined from the Ergun equation for Newtonian fluids. A tentative value for the third parameter is determined from limited experimental data on aqueous solutions of Carbopol 941. The resulting correlation can be used to estimate the pressure drop for flow of a yield stress fluid through a packed bed. A criterion for determining when flow will or will not occur is also deduced.

This correlation is used to model cake filtration of a yield stress fluid for a particular constant pressure drop and particle size. The model results show the dramatic effects the yield stress has on changing the flow rate and cake growth rate from that for a Newtonian fluid.

In its present form the yield stress model is limited to packed beds and filter cakes of spherical particles of monotonic size. Future work should consider effects of size distributions and shapes of particles. Also, more extensive experimental data should be used to refine the value of parameter C_3 in Eq. (32).

NOTATION

C_1, C_2, C_3	Constants in correlations [—]
d_p	particle diameter [m]
F_k	drag force acting of fluid flow acting on a tube wall [N]
F_z^d	interphase drag force [N/m^3]
f	friction factor [—]
f_o, f_∞	friction factor values at low and high Reynolds numbers [—]
g	gravity acceleration [m/s^2]
G	cake volume to filtrate volume ratio [—]
H_e, H_{ep}	Hedstrom number, Hedstrom number for packed bed or filter cake [—]
L	cake height [m]
P, P^f	dynamic and fluid phase pressures [N/m^2]
P_o, P_L	pressure at inlet and outlet of cake [N/m^2]
Q	volumetric flow rate though the packed bed [m^3/s]
R, R_{tube}, R_{bed}	radius, capillary radius, radius of filter cake or packed bed [m]
R_e	Reynolds number [—]
R_{ep}	Reynolds number for packed bed [—]
R_h	hydraulic radius [m]
t	time [s]
$\langle v \rangle$	average velocity in capillary [m/s]
v_z^f, v_z^s	fluid and solid phase velocities in the z-direction [m/s]
V	superficial velocity [m/s]
z	spatial position in the cake [m]
μ	Newtonian fluid viscosity [kg/m/s]
μ_o	fluid phase yield stress modulus [N/m^2]
τ_o	fluid phase yield stress [N/m^2]
τ_{rz}	rz component of the fluid phase shear stress [N/m^2]
τ_R	shear stress at the capillary tube wall [N/m^2]
τ^s	stress on the solid phase matrix [N/m^2]
ε, ε^f	porosity or void volume fraction of the cake [—]
ε_{slurry}^f	fluid phase volume fraction in the slurry approaching the cake [—]

ε^s	solid phase volume fraction [—]
ρ, ρ^f	fluid phase density [kg/m^3]
ρ^s	solid phase density [kg/m^3]

ACKNOWLEDGMENTS

The authors acknowledge their sincere gratitude to BF Goodrich for the donation of the Carbopol 941 and Department of Polymer Engineering of the University of Akron for use of their Dynamic Stress Rheometer.

REFERENCES

1. Shirato, M.; Aragaki, T.; Iritani, E.; Wakimoto, M.; Fujiyoshi, S.; Nanda, S. Constant pressure filtration of power-law non-Newtonian fluids. J. Chem. Eng. Jpn **1977**, *10* (1), 54–60.
2. Shirato, M.; Aragaki, T.; Iritani, E. Analysis of constant pressure filtration of power-law non-Newtonian fluids. J. Chem. Eng. Jpn **1980**, *13* (1), 61–66.
3. Shirato, M.; Aragaki, T.; Iritani, E.; Funahashi, T. Constant rate and variable pressure-variable rate filtration of power-law non-Newtonian fluids. J. Chem. Eng. Jpn **1980**, *13* (6), 473–478.
4. Kozicki, W.; Kuang, P.Q. Cake filtration of suspensions in viscoelastic fluids. Can. J. Chem. Eng. **1994**, *72* (5), 828–839.
5. Kozicki, W.; Slegr, H. Filtration in viscoelastic continua. J. Non-Newtonian Fluid Mech. **1994**, *53*, 129–149.
6. Nassehi, V. Modelling of combined Navier–Stokes and Darcy flows in crossflow membrane filtration. Chem. Eng. Sci. **1998**, *53* (6), 1253–1265.
7. Abbasov, T.; Herdem, S.; Koksal, M. Particle capture in axial magnetic filters with power law flow model. Appl. Phys. D **1999**, *32* (10), 1097–1103.
8. Galeczki, G.; Galeczki, G. Utilization of random porous media (RPM) for studying the flow behavior of red blood cells. Biorheology **1995**, *32* (2–3), 310–311.
9. Ergun, S. Fluid flow through packed columns. Chem. Eng. Prog. **1952**, *48* (2), 89–94.
10. Christopher, R.H.; Middleman, S. Power-law flow through a packed tube. Ind. Eng. Chem. Fundam. **1965**, *4* (4), 422–426.

11. Park, H.C.; Hawley, M.C.; Blanks, R.F. The flow of non-Newtonian solutions through packed beds. Polym. Eng. Sci. **1975**, *15* (11), 761–773.
12. Marshall, R.J.; Metzner, A.B. Flow of viscoelastic fluids through porous media. Ind. Eng. Chem. Fundam. **1967**, *6* (3), 393–400.
13. Hayes, R.E.; Afacan, A.; Boulanger, B.; Shenoy, A.V. Modelling the flow of power law fluids in a packed bed using a volume-averaged equation of motion. Transport Porous Media **1996**, *23* (2), 175–196.
14. Pascal, H. Non-steady flow through porous media in the presence of a threshold gradient. Acta Mech. **1981**, *39* (3–4), 207–224.
15. Al-Fariss, T.; Pinder, K.L. Flow through porous media of a shear-thinning liquid with yield stress. Can. J. Chem. Eng. **1987**, *65* (3), 391–405.
16. Bird, R.B.; Stewart, W.E.; Lightfoot, E.N. *Transport Phenomena*; Wiley: New York, 1960.
17. MacDonald, I.F.; El-Sayed, M.S.; Mow, K.; Dullien, F.A.L. Flow through porous media—the Ergun equation revisited. Ind. Chem. Fundam. **1979**, *18* (3), 199–207.
18. Wünsch, O. Experimentelle bestimmung binghamscher stoffparameter. Rheol. Acta **1990**, *29* (2), 163–169.
19. Foust, A.S.; Leonard, A.W.; Clump, C.X.; Maus, L.; Andersen, L.B. *Principles of Unit Operations*; Wiley: New York, 1960.
20. Patel, R.D. Non-Newtonian flow. In *Handbook of Fluids in Motion*; Cheremisinoff, N.P., Gupta, R., Eds.; Ann Arbor Science: Ann Arbor, MI, 1983; Chap. 6, 135–178.
21. Bear, J. *Dynamics of Fluids in Porous Media*; Elsevier: New York, 1972.
22. Hassanizadeh, M.; Gray, W.G. General conservation equations for multi-phase systems: 1. Averaging procedure. Adv. Water Resour. **1979a**, *2* (3), 131–144.
23. Hassanizadeh, M.; Gray, W.G. General conservation equations for multi-phase systems: 2. Mass, momenta, energy, and entropy equations. Adv. Water Resour. **1979b**, *2* (4), 191–203.
24. Hassanizadeh, M.; Gray, W.G. General conservation equations for multi-phase systems: 3. Constitutive theory for porous media flow. Adv. Water Resour. **1980**, *3* (1), 25–40.
25. Slattery, J.C. *Momentum, Energy, and Mass Transfer in Continua*, 2nd Ed.; Kriegers: Huntington, New York, 1981.
26. Willis, M.S.; Collins, R.M.; Bridges, W.G. A complete analysis of non-parabolic filtration behavior. Chem. Eng. Res. Des. **1983**, *61* (2), 96–109.
27. Chase, G.G. Unified analysis of compressive packed beds, filter cakes, and thickeners. Sep. Sci. Technol. **1992**, *27* (8&9), 1093–1114.
28. Chase, G.G.; Willis, M.S. Compressive cake filtration. Chem. Eng. Sci. **1992**, *47* (6), 1373–1381.